Acoustically driven emission of light in granular and layered semiconductors: recent advances and future prospects

O A Korotchenkov[1], T Goto[2], H G Grimmeiss[3], C Rocke[4] and A Wixforth[4]

[1] Faculty of Physics, Kiev University, Kiev 03680, Ukraine
[2] Department of Physics, Graduate School of Science, Tohoku University,
Sendai 980-8578, Japan
[3] Solid State Physics, University of Lund, Box 118, S-221 00 Lund, Sweden
[4] Sektion Physik and Centre for Nano Science, LMU, Geschwister-Scholl-Platz 1,
D-80539 München, Germany

E-mail: olegk@mail.univ.kiev.ua

Abstract

Acoustic driving techniques can produce luminescence in semiconductors quite efficiently. A mixture of grain particles, for example, emits light when driven by sufficiently intense acoustic fields. This effect is therefore particularly interesting for exploring the dynamics of granular solids. By applying this novel technique, further insight is gained when monitoring the driving-induced evolution of dense particle arrangements. Another subject in this article is the description of the basic physics that governs acoustically driven relaxation of photoexcited carriers in quantum well systems. Due to these properties, μs-prolonged recombination processes and periodic pumping of exciton emission in a quantum dot are observed, which offer new possibilities for tailoring multilayer structures of semiconductors. A variety of potential applications using these phenomena are envisaged.

Contents

1. Introduction

A large variety of information on light emission in sound fields, a phenomenon usually called sonoluminescence, has been obtained for liquids and ionic crystals. The studies have been performed during the last few decades and they continue to be a subject of great interest to physicists, as demonstrated by the large number of recent reviews (e.g. Walton and Reynolds (1984), Crum (1994), Barber *et al* (1997), Ostrovskii *et al* (1999)). The number of systems that exhibit sonoluminescence effects is increasing rapidly and includes now even granular media (Korotchenkov and Goto 1997). There seems to be a lack of consistency in the terminology for such driving effects in solids. Several different designations have been employed for these effects including acoustoluminescence (Ostrovskii 1981) and sonoluminescence (Ostrovskii and Das 1997, Korotchenkov and Goto 1997). Here, we use the term 'acoustically induced' luminescence if the acoustic driving itself yields emission of light, whereas the term 'acoustically driven' luminescence is applied when the driving affects the photoexcited luminescence of semiconductors.

It is not our intention to present in this article a detailed summary of results obtained on acoustically induced luminescence effects in crystals and liquids, since every aspect of these phenomena including the light-emission mechanism seems to have been extensively discussed in the above reviews. Instead, we shall focus our discussion on the latest studies on the nature of emission of light in granular substances. Two different cases, namely cavity-QED-enhanced (QED being quantum electrodynamics) spontaneous emission from collapsing voids between grains (Prevenslik 2000) and hot-electron radiation in conjunction with defect luminescence (Ostrovskii and Korotchenkov 2000), will be of particular interest.

The discovery of acoustically induced luminescence in granular substances seems to be an unusual and fascinating subject, not only due to the unique properties of granular materials themselves (Jaeger *et al* 1996), especially in connection with the enormous richness and complexity of granular motion, but also because of its potential application in materials science and processing techniques (Korotchenkov and Goto 1999). Certain specific aspects of this latter paradigm will be emphasized in the article. Hence, another goal of this review is to provide the current state of knowledge on granular dynamics as demonstrated by acoustically induced luminescence techniques.

A further subject emphasized in this review is the acoustically driven luminescence of excitons in semiconductor quantum wells. It is well known that the exciton localization at random potentials and their quantum confinement in low-dimensional structures quite considerably increases the importance of excitons in optical absorption and photoluminescence (PL) processes. The established model of exciton formation and radiative recombination distinguishes between free (or delocalized) and localized excitons, implying that a dynamic equilibrium is established between excess free carriers and excitons. Compared with recombination of free carriers, excitonic recombination is thus expected to increase when the temperature is lowered. Hence, at low temperature, the near-band-edge PL is usually dominated by excitonic transitions. Moreover, since the carriers form excitons they cannot contribute to photoconductivity, which suggests that the generation of excitons also has an impact on photoconductivity measurement techniques.

It is therefore not surprising that excitons have been the subject of increasing interest for many years and consequently have generated numerous publications. One of the goals of this review is to discuss the recent excitement about acoustic driving effects on radiative recombination of excitonic processes in quantum wells (Rocke *et al* 1997, 1998, Korotchenkov *et al* 1999, Streibl *et al* 1999, Santos and Hey 2000, Sogawa *et al* 2001). Whereas the impact of electric or magnetic fields on excitonic luminescence is quite significant and rather well known
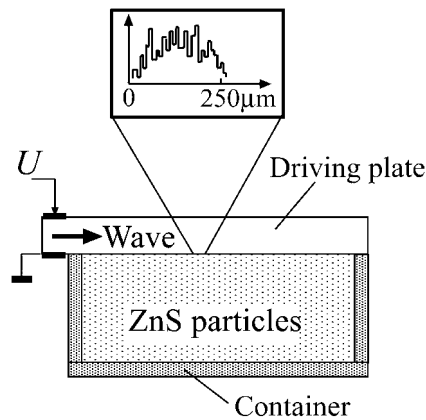
Figure 1. A schematic side view of the acoustic cell used for the observation of acoustically induced luminescence in ZnS grain mixtures. The rf driving voltage U in the MHz range is applied to the LiNbO$_3$ piezoelectric plate. The container confines ZnS particles in a mm-sized bed. The light emission discussed in section 2.2 is imaged in a 0–250 μm illuminating spot.

(e.g. Mendez *et al* (1982), Polland *et al* (1985), Aksenov *et al* (1995)), related phenomena including electric fields and deformation potentials of acoustic waves are not adequately understood. Surface acoustic waves (SAW), i.e. surface vibrations of a solid, generated in piezoelectric semiconductors like ripples on water, are therefore of particular interest for our presentation, which will also include waves propagated in plates. The plate geometry is capable of generating unlimited numbers of vibration modes, allowing multi-branched frequency spectra of transmitted waves. Papers on surface waves and wave motions in plates have previously been published by Viktorov (1967), Auld (1990) and Graff (1991). The influence of the piezoelectric potential of acoustic waves on the electron–hole pair recombination starts as soon as the wave propagates across the solid with quite a small attenuation. Why and how this happens constitutes one of the subjects in this article.

Insight into the basic physics of acoustically driven luminescence in low-dimensional systems will facilitate the exploitation of this new technology. It is therefore our intention to present a few qualitative considerations on the basic features of acoustically driven lasing effects in semiconductor microcavities (Wiele *et al* 1998). We hope that these considerations will stimulate a new thinking in band-gap engineering by employing superlattices that are acoustically modulated in the plane of a quantum well and start a discussion on a number of interesting features of acoustically driven delay of photonic signals (Rocke *et al* 1997, Zimmermann *et al* 1999).

The article is organized as follows. Section 2 discusses acoustically induced light emission in granular mixtures of semiconductor microcrystallites. Section 3 describes acoustically driven luminescence of excitons in quantum well structures. Section 4 outlines a variety of possible applications together with some unresolved problems.

2. Acoustically induced luminescence in granular media

Light emission has been observed in a mixture of micron-sized ZnS particles which has been induced by sufficiently intense ultrasonic Lamb waves of MHz frequency travelling in a driving plate of piezoelectric LiNbO$_3$; see figure 1 (Korotchenkov and Goto 1997). The mixture of vertical and horizontal displacements at the surfaces of the plate (Viktorov 1967), and the appearance of a steady force (Nyborg 1965), which accompanies the travelling wave at the boundary and in the interior of the grains, produces a complicated particle velocity field near the driving plate. Since the wavelength of propagation is typically of the order of 100 μm, the spatial period of the stress can easily span 50–100 grain lengths. Hence, there is no reason to believe that the mixture of ZnS grains remains homogeneous.
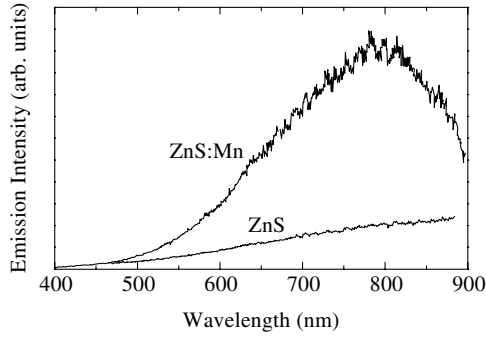
Figure 2. Spectra of acoustically induced luminescence from ZnS:Mn and ZnS grains (Korotchenkov and Goto 1997). Using a driving voltage of $U \approx 70$ V, the total radiance is roughly 10^{-13} W and 0.2×10^{-13} W in doped and undoped mixtures, respectively.

It is known that a random assembly of spherical particles can be packed with a packing density from $\eta = 0.55$ to 0.64 (Onoda and Liniger 1990, Bideau and Dodds 1991), depending on the preparation procedure of the grain mixture. The phenomena discussed here involve values of η that are even smaller, of the order of 0.4 for randomly packed nonspherical particles (Korotchenkov and Goto 1999). In first approximation, it is therefore fair to say that external driving forces induce particles slipping to available slots, allowing the system to attain randomly densified arrangements. This leads to a fundamental issue concerning the packing of ZnS particles when driven by acoustic waves. If we assume that mixture densification occurs randomly above some threshold value of the driving stress so that the emitted light is closely linked to granular motion, then the physics behind acoustically induced emission of light is governed by granular dynamics.

2.1. Defining light-emitting mechanisms

Several different models such as frictional electricity, Planck's theory, and grain collision-induced emission, have been proposed to explain the observed emission of light in granular media. For the discussion of light-emitting mechanisms, it is appropriate to use spectral studies, since correct predictions of the measured spectra is a minimum requirement for the proposed model.

Although frictional electricity has often been used in describing mechanically induced light emission (see, e.g., the historical survey by Walton (1977)), spectral data have shown serious weaknesses in explaining acoustically induced luminescence by this mechanism, considering that the spectra emitted by acoustically driven grains are broad and continuous; see figure 2. These spectra are rather different from the line spectrum of microdischarges in ambient gas which are generally observed in the luminescence of frictional electricity (Picard 1676, Langford *et al* 1987).

Other explanations for the light-emitting mechanism employ ideas from cavity quantum electrodynamics (see the review by Haroche and Kleppner (1989)). The original idea of a 'QED route' to sonoluminescence is due to Schwinger (1992) and was vividly discussed in the 1990s (e.g. Eberlein (1996), Colic and Morse (1998), Visser *et al* (1999)). Figure 3(*a*) illustrates a typical cavity-QED arrangement implying an atom that is confined between two plates separated by ξ. The spatial distribution of the electromagnetic field is controlled by the plate arrangement and exhibits a dramatic change of the mode structure of the field when the cavity size becomes comparable to the wavelength, $\lambda = 2\xi$. For optical fields, the cavity structure consists of a micron-sized spacing.

This idea has been used to explain acoustically induced luminescence in granular media. In what follows we summarize the original discussion of Prevenslik (2000). Figure 3(*b*) shows
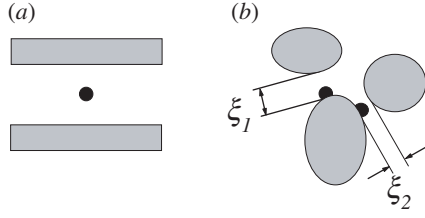
(a)   (b)

Figure 3. One atom (closed circle) placed in the cavity between two dielectric plates (*a*) and two atoms placed on the grain surfaces (*b*).

three grain particles which illustrate the complicated geometry of voids between grains. As the cavity QED requires the frequency of the spontaneous emission of atoms on the grain surface to coincide with the frequency of the standing-wave resonance, the confined spaces between grain surfaces contain electromagnetic waves of energies

$$E_k = \frac{hc}{\lambda_k} = \frac{hc}{2\xi_k}. \tag{2.1}$$

Here, h is Planck's constant, c is the velocity of light, and λ_k is the wavelength of the kth wave corresponding to the void between grains that are separated by ξ_k. It is further postulated that the spectra as exemplified in figure 2 originate from a cavity-QED-enhanced spontaneous emission due to confined spaces ξ_k. The voids, which are initially widely separated, are supposed to grow and to collapse periodically in acoustic fields. Fitted spectra are then easily obtained by taking the statistical distribution of ξ_k.

In this simple model it is further assumed that the grains are spherical with radius r and identical, so that the volume per grain in a mixture is

$$\overline{V} = \frac{4}{3}\pi \left(r + \frac{\xi}{2}\right)^3. \tag{2.2}$$

Then the packing density is given by

$$\eta = \frac{4\pi r^3}{3\overline{V}} = \frac{1}{(1 + \xi/2r)^3}. \tag{2.3}$$

We can calculate the emission intensity through $I \propto E_k W_k$ where W_k the probability for the occurrence of the intergrain separation ξ_k. If we take

$$W_k = \exp\left[-\frac{1}{2}\left(\frac{r_k - \overline{r}}{\delta}\right)^2\right] \tag{2.4}$$

with $\overline{r}$ the average grain radius and δ the standard deviation and put ξ from equation (2.3) into the photon energy given by equation (2.1), we obtain for the expected spectrum of a grain mixture

$$I = \frac{hc}{4r_k\left(\eta^{-1/3} - 1\right)} \exp\left[-\frac{1}{2}\left(\frac{r_k - \overline{r}}{\delta}\right)^2\right]. \tag{2.5}$$

Equation (2.5) relates the wavelength content of the emission spectrum to the size distribution of the powder grains. Taking $\overline{r} = 1.5$ μm and $\delta = 0.2$ μm (Prevenslik 2000), it has been suggested that about the same wavelength dependence should exist in the fitted spectra as in the experimental data. Properly fitted curves (curve 1 in figure 4) are indeed in good agreement with experimental results (points in figure 4). However, more recent measurements show that the above value of δ is possibly overestimated. Using data obtained by Korotchenkov and Goto (1999), we have reason to believe that a more appropriate value of δ is 0.11 μm. Using equation (2.5), we find that the calculated spectrum (curve 2 in
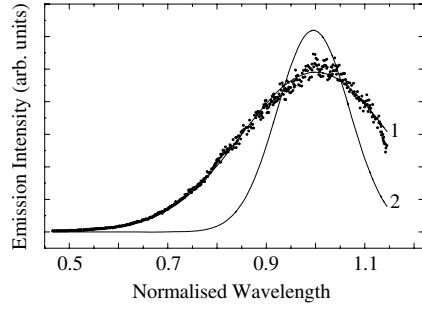
Figure 4. The wavelength dependence of the measured emission spectrum in ZnS:Mn grains from figure 2 (circles) and the best-fitting spectra obtained by using equation (2.5) (lines) for $\delta = 0.2$ μm, $\bar{r} = 1.5$ μm (curve 1) and $\delta = 0.11$ μm, $\bar{r} = 1.5$ μm (curve 2). The wavelength is normalized to the maximum position of the measured spectrum.

figure 4) comprises an emission band which is considerably narrower than the one observed in experiment. Furthermore, by taking values for ξ between 0.5 and 1.2 μm as typical values of intergrain separations (Korotchenkov and Goto 1999), one would expect the peak of the emission band, at least for the ZnS:Mn grains, at higher wavelengths than in figure 2.

Therefore, although the cavity-QED hypothesis provides a consistent explanation for the broad-band spectrum of emitted light, it should be noted that full calculations taking into account further details of the model have not been performed. Experiments which relate the spectral distribution of the emission to precisely determined grain and intergrain parameters are therefore needed to find out which of the mechanisms discussed is responsible for the observed emission.

A completely different explanation has been suggested for the light-emitting mechanism— by interpreting the broad-band spectrum as radiative emission of hot electrons in the conduction band (Ostrovskii and Korotchenkov 2000). A similar approach has been used to explain the broad-band electroluminescence spectra in ZnS Schottky diodes which extend from the visible to the near infrared region (Rigby and Allen 1988). In this connection, the important question is whether or not carrier heating does indeed occur in acoustic fields. In the absence of direct experimental evidence, this effect may well be of importance due to the fact that the driven grains collide rather heavily. Electrons may therefore be excited in the grains both due to thermal excitation and due to high electric fields generated near the surface of the grains. Hence, mechanical interactions between grains themselves and grains and the driving plate should be important processes for generating the emission (Korotchenkov and Goto 1997).

An estimation of the electric field strength can be performed in order to obtain a simple quantitative prediction of the maximum field strength, which may illustrate the validity of the suggested model. Many theoretical and experimental studies have been reported on the interaction of contacting bodies with respect to the deformations, which arises in the contact region, and the kinetics of the stresses generated in the particles (Landau and Lifshitz 1986, Thornton 1993, Thadhani et al 1997). The mode of deformation depends rather sensitively on the impact velocity of the grains. As the impact velocity is increased, more kinetic energy goes into irreversible work deforming the particle surfaces in the contact region. Eventually, an all-plastic situation is reached. Let us suppose that, up to the instant of a maximum compression, the kinetic energy of colliding particles is absorbed in local elastic deformations of the grains and that

$$\frac{mV^2}{2} = \frac{CS^2 \upsilon}{2} \tag{2.6}$$

where m is the mass of a grain, V is the impact velocity, C is the elastic constant of the material, S is the strain generated in the impact and υ is the volume of the grain. Taking $m = \rho \upsilon$ with ρ the density of the grain, we then equate
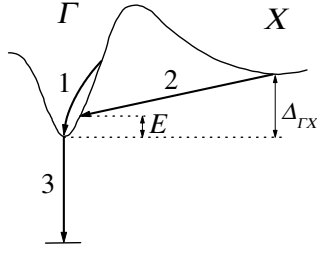
Figure 5. A schematic diagram of the transitions within the Γ and X valleys in the band structure (1 and 2) as well as defect-related radiative recombination (3) used to explain the spectra of acoustically induced luminescence in ZnS powders.

$$S = V\sqrt{\frac{\rho}{C}}. \tag{2.7}$$

Furthermore, the following approximation has been proposed to describe the dependence of the grain velocity on the amplitude A for the surface motion of the driving plate (Korotchenkov and Goto 1997):

$$V = 2\pi f A \tag{2.8}$$

where f is the frequency of acoustic waves in the driving plate. According to Ostrovskii *et al* (1999), the wave amplitude is typically $A \sim 1$ nm and, hence, the impact velocity is $V \approx 0.03$ m s^{-1} at $f = 5$ MHz. This gives $S \sim 6 \times 10^{-6}$.

Zinc sulphide is known to exist in two modifications and both of them are piezoelectric. Taking the piezoelectric constant $\epsilon \approx 0.15$ C m^{-2}, the magnitude of the electric field strength, imposed by the impact, is $F \sim S/\epsilon \approx 4 \times 10^{4}$ V cm^{-1}. Fields of this size are often used to achieve free-carrier heating (see e.g. Pankove (1971)), which strongly supports the light-emitting mechanism outlined above. However, it should be stressed that the estimate that we made obviously only accounts for the average magnitude of the generated field. For a good understanding of the dynamic response of the grain subjected to a rapid loading, it is important to accurately account for the maximum field strength attained during the impact. Given the importance of an accurate determination of the time evolution of the initially overstrained contact region of the grain, it is, hence, desirable to take into account even the initial strain jump in the deformed zone. It can therefore not be excluded that even higher values of the field strength than that obtained in our simple estimation can be achieved in the near-surface regions of the grains.

In fact, the broad emission bands seen in figure 2 could be generated by a combination of intravalley and intervalley indirect radiative transitions of electrons as illustrated by arrows 1 and 2 in figure 5 for the Γ and X valleys in the conduction band. These electrons are excited by gaining energy through the mechanical interactions of the grains near the driving LiNbO$_3$ plate and occupy higher-energy states in the conduction band. Inelastic grain interactions are likely to exert high pressures, electric fields and thermal effects in the near-surface regions of the grains, thus constituting the mechanism of free-carrier excitation. The validity of this model is checked by a closer inspection of the spectral distribution.

Assuming a Maxwellian distribution of the carriers in the parabolic Γ valley, we can readily calculate the emission spectrum produced by the electronic transition 1 in figure 5 through

$$I \propto \exp\left(-\frac{h\nu}{kT}\right) \tag{2.9}$$

where ν is the photon frequency, k is Boltzmann's constant and T is the effective electron temperature. Figure 6 shows experimental emission data in a semilog plot which have been
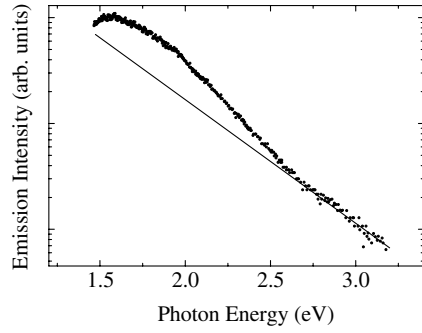
Figure 6. The wavelength dependence of the measured emission spectrum for ZnS:Mn grains from figure 2 on a semilog scale (circles) and the exponential fit (line) to the higher-energy side of the spectrum.
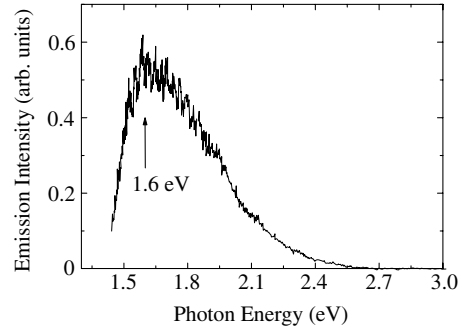
Figure 7. The difference of the measured emission spectrum and the fitted exponential spectrum exhibited in figure 6.

observed for ZnS:Mn grains. These data can be fitted by equation (2.9) in two different ways. For reasons which will become clear later, we fitted the high-energy part of the emission band (the line in figure 6) and obtained an electron temperature as high as 4000–4500 K.

At this point, two comments are in order. Firstly, the linear fit exhibited in figure 6 suggests that such a fit may also be applicable to conduction-to-valence band radiative transitions. Since the distribution of free electrons in the conduction band is of a similar type to the one shown as equation (2.9), the high-energy part of the interband recombination is expected to be linear in a semilog plot. However, emissions of this type should have a low-energy threshold close to the energy gap. Considering that the energy gap of ZnS is 3.6 eV at room temperature, it is therefore unlikely that the high-energy part of the spectrum displayed in figure 6 is due to interband radiative transitions. This is still true, even if many-body interactions of photons and electrons are taken into account (Ryvkin 1965), which may decrease the photon energy of the emitted light. Secondly, momentum conservation rules will reduce the probability of radiative recombination processes quite considerably. Due to the low transition probability, the observed emission is rather weak and could only be observed in the dark, as pointed out previously (Korotchenkov and Goto 1997). Furthermore, in pure samples additional phonons are needed to complete the transitions, which implies that the emission intensity for undoped ZnS powder is considerably smaller than the one for ZnS:Mn grains, as shown in figure 2. It is therefore not unreasonable to assume that transition 1 in figure 5 is due to radiative scattering at ionized defect centres which relaxes the momentum conservation rules.

There is also a remarkable deviation from the calculated spectrum on the low-energy side of the spectrum shown in figure 6. This deviation suggests that the observed spectrum most probably is not described by a pure intravalley electron transition (1 in figure 5) but rather by a convolution of at least two processes. In order to obtain more information on the superimposed band, the difference between the experimental points and the linear fit shown in figure 6 is plotted in figure 7. It is worth mentioning that highly Mn-doped ZnS phosphors display emission spectra peaked between 1.5 and 1.6 eV. These peaks have been tentatively ascribed to optical transitions involving intrinsic defects, although the nature of these defects is not definitely known (Tong and Goede 1983). It seems therefore quite reasonable to assume (see Korotchenkov and Goto (1997)) that the band peaked at 1.6 eV in figure 7 is due to defect-related emissions (transition 3 in figure 5) involving transitions of electrons from the conduction band into deep-lying states in the forbidden energy gap. For this reason, the high-energy and not the low-energy part of the emission band in figure 6 was fitted by equation (2.9).

The next question is that of whether the two transitions 1 and 3 (see figure 5) are the only likely ones which explain the observed emission. To answer the question, Ostrovskii and Korotchenkov (2000) pointed out quite recently that radiative transitions of hot electrons between different valleys of the conduction band (transition 2 for the X and Γ valleys in figure 5) should be taken into account in analogy with previous observations (Turvey and Allen 1973, Rigby and Allen 1988). Such transitions are only allowed when the momentum is conserved, e.g. by impurity or phonon scattering, and lead to a broad emission spectrum with a high-energy cut-off corresponding to the intervalley separation. The spectral dependence of these transitions can be approximated by

$$I(h\nu) \propto M^2 g(E) w(E) \tag{2.10}$$

where M is the matrix element of the transition, $g(E)$ is the density of states in the Γ valley, $w(E)$ is the probability that the state in the conduction band corresponding to $h\nu$ is not occupied and $E = \Delta_{\Gamma X} - h\nu$. Suppose electrons excited in the upper valleys of the conduction band only populate states in the higher band minima where the effective mass is large. If the lower valley has a small effective mass, the change of the wavevector accompanying the electron transition of energy $\Delta_{\Gamma X}$ is constant. The same is valid for the transition matrix element M in equation (2.10). The shape of the spectrum near the cut-off energy is then determined by the density of states in the lower valley (Turvey and Allen 1973). Assuming $g(E) \propto \sqrt{E}$ near the bottom of the Γ branch, the emitted spectrum is given by

$$I(h\nu) \propto \sqrt{\Delta_{\Gamma X} - h\nu}. \tag{2.11}$$

This implies that the high-energy limit of the emission spectrum is expected to correspond to the X–Γ spacing. As pointed out by Ostrovskii and Korotchenkov (2000), the cut-off energy at about 2.6 eV for the spectrum in figure 7 agrees reasonably well with previous calculation of the X–Γ separation (Czyzyk and Mueller 1983). Using the $g(E)$ calculations of Huang and Ching (1993), a peak energy of 1.67 eV is derived for the spectrum $I(h\nu)$ which is in close agreement with the one exhibited in figure 7. Hence, the emission exhibited in figure 7 could be due to both the transitions 2 and 3 in figure 5. In order to find out which of these transitions is dominant, one has to take into account the broad-band nature of the observed emission (spectra in figure 2), and the fact that the prominent PL bands of the yellow emission observed for ZnS:Mn grains and the blue self-activated emission band for ZnS particles (Korotchenkov and Goto 1997) are not observed in the spectra exhibited in figure 2. Since the Mn ion is known to act as a highly effective luminescence centre, it seems unlikely that the observed emission is generated in the interior of the grain and that the observed light is mostly due to luminescent defect centres. It is therefore assumed that the emission originates from regions close to the surface. The observed broad spectra are at least partly due to electrons which have been heated by grain impacts and transferred to the upper states of the conduction band, this being followed by radiative transitions to the lowest states within the Γ valley.

The good agreement with experimental results obviously suggests that the model of acoustically induced luminescence shown in figure 5 is more likely than the one presented in figure 3(b). However, additional experiments are needed for a better understanding of light emissions due to acoustically driven grains.

2.2. Capturing dynamics of vibrating powders

Regardless the final model of light emission, the preceding examples rather clearly illustrate that the observed emission is evidence of an underlying interaction of closely packed particles and, hence, that it should be helpful for a better understanding of the process used to monitor the driving-induced evolution of dense particle arrangements. In this respect, CCD-camera
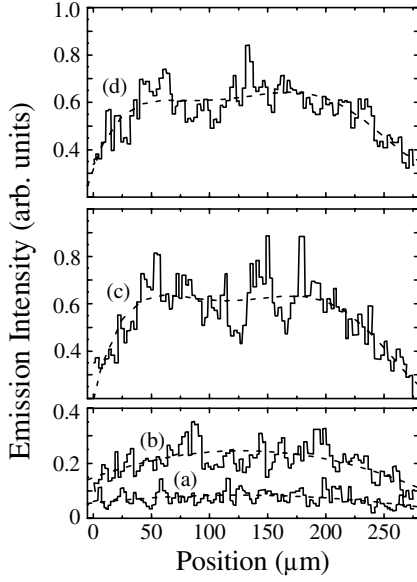
Figure 8. Evolution of the emission intensity cross section with driving amplitude at a given location on the illuminated surface (figure 1) of more packed ZnS:Mn grains ($\eta \approx 0.43$). Panels (a), (b), (c) and (d) are taken at U denoted by arrows a, b, c and d, respectively in figure 10 (closed circles). After Korotchenkov and Goto (1999).
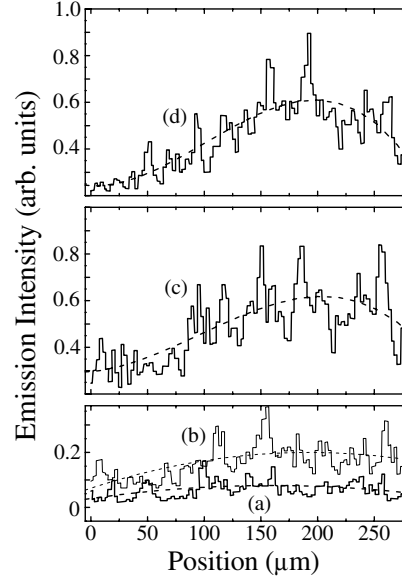
Figure 9. The same evolution as in figure 8, but with the grain mixture prepared under less packed initial conditions ($\eta \approx 0.37$). Panels (a), (b), (c) and (d) are taken at U denoted by arrows a, b, c and d, respectively (open circles), in figure 10. After Korotchenkov and Goto (1999).

imaging is particularly useful because this technique can be used to image small emitting patterns with a spatial resolution close to the diffraction limit of visible light (~ 1 μm). The bright surface of a mixture of grains is characterized by spatially distributed spots that were imaged to produce two-dimensional snapshots of the surface colour (Korotchenkov and Goto 1997). The driving-induced evolution of the surface colour can then be serially monitored to observe the evolution of arbitrary cross sections of emission intensities which is a prerequisite for studying grain dynamics. Cumulative studies of acoustically induced luminescence are very helpful in developing these new techniques, which offer new possibilities for studying such luminescence phenomena and a better understanding of general trends.

One example supporting this view is shown in figures 8–10 for the case of more ($\eta \approx 0.37$) and less packed ($\eta \approx 0.43$) starting mixtures of grains. The intensities taken in the areas of enhanced emission appear to be roughly uniform at low driving amplitudes (figures 8(a) and 9(a)), corresponding to the region ab for the computed total image emission intensity versus U in figure 10. At higher driving, when the driving plate is energized by values of U corresponding to the region bd of figure 10, the emitting patterns are essentially inhomogeneous ((b)–(d) in figures 8 and 9). It is interesting to note that the average emission intensity exhibited by dashed curves in figures 8 and 9 reveals a considerably sharper increase over the illuminating pattern in more packed mixtures ((b)–(d) in figure 8) than in less packed mixtures ((b)–(d) in figure 9). Secondly, the largest variations in the emission intensity, shown by the solid lines in figures 8 and 9, occur across emitting patterns that achieve the greatest values in figures 8(c) and 9(c). At higher driving, above point c in figure 10, variations in emission intensities are considerably more suppressed in more packed mixtures (figure 8(d)) than in less packed mixtures (figure 9(d)).
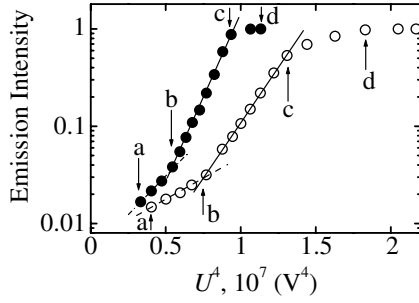
Figure 10. Logarithm of emission intensity I as a function of U^4. Solid and dashed lines indicate fits to equation (2.16) by using data points at which they intersect (after Korotchenkov and Goto (1999)).

The precise functional form of the total emission intensity I versus driving voltage U is unknown. For our purpose, we may use the kinetic theory approach to granular flow (Haff 1983, Jenkins and Savage 1983). Within the framework of this simplified model, the pressure exerted by the driving LiNbO$_3$ plate is given by

$$p \propto \frac{\Delta K}{\tau_{\text{col}} (2r)^2} \tag{2.12}$$

where $\Delta K \propto mV$ is the momentum transfer in a collision of two grains, $\tau_{\text{col}} \propto \xi/V$ is the grain collision time and V is the average velocity of a grain near the plate. We then calculate the pressure p through

$$p \propto \frac{U^2}{\xi} \tag{2.13}$$

where U is the driving voltage amplitude (see figure 1). In writing equation (2.13), we have assumed that the grain velocity obeys the law

$$V = 2\pi f A \propto U. \tag{2.14}$$

The simplest assumption consistent with the implied grain collision-induced hypothesis of the production of light is that the emission intensity I is related to the pressure p by

$$\ln I \propto p^2 \tag{2.15}$$

which has previously been observed for the pressure-induced luminescence of ZnS phosphors (Alzetta *et al* 1962). Expressions for acoustically induced emission intensities can then be approximated in terms of the grain velocity and the voltage applied to the driving plate:

$$\ln I \propto \frac{V^4}{\xi^2} \propto \frac{U^4}{\xi^2}. \tag{2.16}$$

It seems rather reasonable that it is indeed the relaxation of density gradients (dashed curves in figures 8 and 9) and particle velocity distributions (solid lines in figures 8 and 9) that give rise to the behaviour that we are describing. Thus, the occurrence of agglomeration patterns with enhanced particle packing at acoustic driving leads to a considerable reduction in grain velocities V, which eventually leads to decreasing emission intensities with increasing driving voltage U (from equation (2.16)) and explains the saturation of the emission intensity exhibited in figure 10 above point c.

Returning to the set of experiments indicated in figures 8 and 9, we encounter a certain analogy: the reduction in V will evidently be most important for denser starting arrangements of the particles, i.e. for a more packed mixture. Consequently, a greater suppression of the rapidly varying emission intensity is observed at high driving in a more packed mixture (solid line in figure 8(d)) compared to that in a less packed mixture (solid line in figure 9(d)). Furthermore,

as the reduction of grain velocities has greater effect in a more packed mixture, this would cause the emission intensity to rapidly saturate at sufficiently high driving. In contrast, a more gradual saturation of the emission intensity is expected in a less packed mixture. This obviously accounts for the difference between the two curves in figure 10 above points *c*. Moreover, we conclude from the preceding discussion that the emission intensity rapidly increases at a distance of about 50 μm across the emitting pattern in a more packed mixture (dashed lines in figures 8(c) and (d)) whereas the more gradual enhancement observed at a distance of about 200 μm is seen in a less packed mixture (dashed lines in figures 9(c) and (d)). This may again be explained by the qualitative picture given above.

Indeed, the viscosity movement of grains would lead to a rapid compaction of more packed mixtures across the wave axis with a subsequent rapid enhancement in the average emission intensity due to the rapid decrease in ξ (see equation (2.16)). The driving-induced grain movement is probably greater in a less packed mixture compared with that in a more packed mixture, thus explaining a gradual increase in the average emission intensity across the pattern seen in figures 9(c) and (d).

The kinetic aspects of the mechanism hypothesized here can be checked experimentally by analysing the evolution of the emission intensity both spatially integrated and spatially resolved after the drive is suddenly switched on and off. Results recently reported by Korotchenkov and Goto (1999) illustrate that the dense particle arrangements produced in acoustic fields relax only gradually with time, thus resembling the problem of packing in a vibrating bed.

Summarizing, we conclude that the measurement technique presented here does indeed make vibrational excitations in granular media accessible.

3. Acoustically driven PL in quantum wells

3.1. Influencing radiative decays of excitons

Since the exciton relaxation processes in quantum wells are our prime concern, we will first present a simple picture which is designed to predict how these processes can be affected by acoustic driving. The kinetics of exciton formation and recombination in QW systems has been extensively studied in recent years (Hegarty *et al* 1982, Feldman *et al* 1987, Ridley 1990, Zachau *et al* 1991, Runge *et al* 1995, Umlauff *et al* 1998). In situations in which excitons are not screened out, photoexcited electrons and holes tend to form excitons rather rapidly. These delocalized excitons relax and lose kinetic energy by inelastic scattering, which implies that the relaxation time for this process is typically of the order of 100 ps as obtained from the rise time of the PL (Damen *et al* 1990). Subsequently, the relaxed excitons either decay radiatively or are converted into localized excitons by being trapped in potential fluctuations.

Let L_z be the quantum well width, where the subscript z refers to the direction normal to the QW plane, i.e. to the xy-plane. When L_z is decreased to about 100 Å, discrete levels are developed from bulk allowed valence and conduction bands due to size quantization. On decreasing the thickness of a QW, the energy gap increases approximately as $\Delta_{QW} \propto L_z^{-2}$. The presence of electrons and holes gives rise to excitonic states with the exciton binding energy E_{ex} exhibiting changes due to spatial fluctuations of the local well width ($E_{ex} \propto a_B^{-2}(L_z)$, a_B being the exciton radius) and a heterointerfacial disorder; see figure 11. The variation of the binding energy and the coherence length L of the exciton causes the luminescence decay constant τ_{PL} to change as (Feldman *et al* 1987)

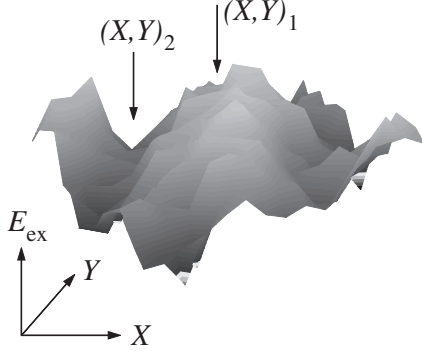$$\tau_{PL} \propto \frac{1}{E_{ex}L^2}. \tag{3.1}$$

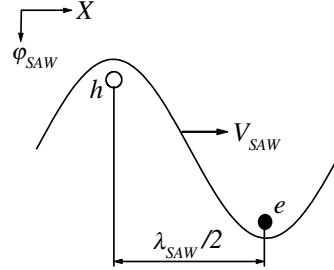**Figure 11.** A schematic picture showing the spatial fluctuation of E_{ex} in the xy-plane of a quantum well.

Figure 12. An illustrative picture showing the storage of photoexcited electrons (e) and holes (h) in the moving piezoelectric potential φ_{SAW} of the SAW.
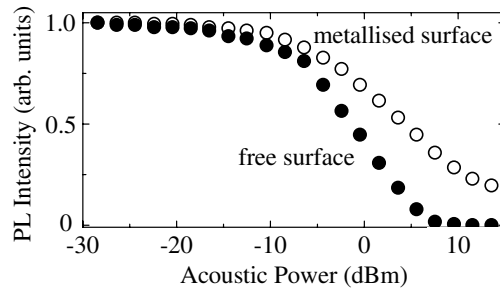

Figure 13. Time-integrated intensity of the exciton PL peaked at about 1.368 eV in a single 10 nm wide InGaAs/GaAs QW structure as a function of the applied acoustic power (a description of the typical experimental device which has been used to provide the driving effect can be found in Tabib-Azar and Das (1987) and Wixforth *et al* (1989)). The IDT is operating at a centre frequency $f_{SAW} = 840$ MHz. The screening of the lateral piezoelectric fields by the semitransparent metallized layer results in a partial recovery of the PL signal.

There is always a local minimum at $x = x_1$ (see figure 11) contributing to a radiative transition of energy $h\nu_{ex} = \Delta_{QW} - E_{ex}(x_1)$, implying that the resulting PL spectrum broadens on the high-energy side. If this is the global minimum of E_{ex} (at $x = x_2$ in figure 11), it determines the low-energy side of the PL spectrum.

It is rather evident from this schematic picture that localized excitons may relax by phonon-assisted tunnelling or thermally activated hopping between localized sites, and that the exciton relaxation can be described by a diffusion formalism (Powell and Soos 1975, Ridley 1990, Runge *et al* 1995). The following question then arises: how can the acoustic driving vary the exciton relaxation, and, in particular, the exciton recombination kinetics? If the moving piezoelectric potential φ_{SAW} of the SAW is increased, the excitons polarize and finally dissociate into individual electrons and holes suppressing the exciton luminescence. The free carriers are separated at most by half a wavelength of the SAW, $\lambda_{SAW}/2$, as shown in figure 12 and transported by the travelling wave propagating along the plane of a QW. On employing a multi-frequency interdigital transducer (IDT) and considering the PL quenching shown in figure 13, the acoustic nature of the driving effect becomes quite evident. As the frequency is varied, the decrease of the PL signal directly maps the frequency response of the IDT. To mediate between the influences of the different piezoelectric field polarizations, a thin
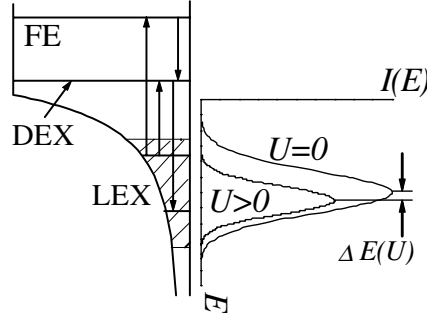
Figure 14. Levels of localized (LEX) and delocalized (DEX) excitons, as well as free electrons (FE) in the potential well approximated by a QW background and a trapping potential well. The resulting PL spectra $I(E)$ are centred around the energy of a nominally deep localized state. The hatched area illustrates the distribution of localized states in the well (Korotchenkov *et al* 1999).

semitransparent metallized layer can be placed on part of the sample which readily screens the lateral components of the field imposed by the SAW. The screening results in a partial recovery of the exciton luminescence as indicated in figure 13.

In the most general case, the acoustic driving effect is quite complex and the localized excitons may be partitioned into detrapped mobile states and spatially separated electrons and holes, as illustrated by upward-pointing arrows in figure 14. These mobile carriers are then free to diffuse and to drift in the moving electric field of the SAW, until they become trapped and relocalized in lower-energy states (downward-pointing arrows in figure 14) with a subsequent increase in the binding energy E_{ex}. If the trapping probability is low, the most important consequence is that the mobile carriers have a chance of being transported over macroscopic distances. Deliberate screening of φ_{SAW} then restores electron–hole pairs into excitons which triggers the radiative recombination and allows μs-prolonged recombination times. Without screening, the excitons change their spectral distribution when relaxing to lower energy (spectra $I(E)$ in figure 14) and the PL decay is effectively varied by the driving. This issue divides the domain of acoustically driven exciton luminescence effects into two qualitatively extreme cases and both have recently been addressed by Rocke *et al* (1997) and Korotchenkov *et al* (1999).

We now turn from our somewhat abstract considerations to a few examples which highlight specific properties of acoustically driven luminescence of excitons in QW systems. Let us first consider the case when the PL in ZnSe/ZnS and InGaAs/GaAs QWs is driven by a piezoelectric field of the SAW. We start by considering three identically grown samples that contain ZnSe single QWs, three, five and seven monolayers (ML) thick, sandwiched between ZnS cap and barrier layers (Yao *et al* 1991). As expected, the peak position and the width of the time-integrated luminescence are dependent on the QW thickness. Thus, the peak energy $h\nu_{ex}$ increases with decreasing well width L_z, as does the PL peak width; the latter observation could well be a consequence of the fact that energy fluctuations of localized excitons resulting from enhanced heterointerfacial disorder are much larger in thinner QWs than in thick ones.

How the driving field leads to the quenching of the PL lines is illustrated in figure 15. The figure compares the time-integrated PL intensity in the 5 ML QW as a function of the driving amplitude for two different excitation energies: 4.0 eV (closed circles) and 3.5 eV (open circles). The key point of this experiment is the fact that the first photon energy is above the band gap of ZnSe (2.8 eV) and ZnS (3.8 eV), while the second energy is smaller than the one needed to optically generate free carriers in ZnS layers.

At least two dominant mechanisms can be proposed to explain the quenching effect. The first mechanism involves thermal effects of the driving that could lead to thermal ionization
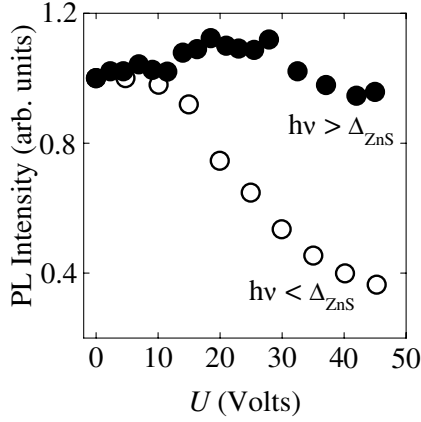
Figure 15. Time-integrated PL intensities of the 5 ML QW versus driving amplitude. The PL has been excited by photon energies of 4.0 eV (closed circles) and 3.5 eV (open circles), respectively (Korotchenkov *et al* 1999).

of excitons. Recent studies tried to clarify the role of the heating effect in acoustic driving techniques (Ostrovskii and Lysenko 1982, Korotchenkov and Grimmeiss 1995, Rocke *et al* 1997, Zhuravlev *et al* 1997, Korotchenkov *et al* 1999) and showed that this mechanism may not be relevant in experiments in which special care is taken to avoid sample heating. Thermal quenching of excitons is expected to be independent of the energy of the exciting light. However, comparing the closed and open measurement points in figure 15, it is quite evident that this assumption is not in agreement with the experimental observations.

The second mechanism is based on the assumption that the driving electric field suppresses the PL. A variety of methods have been applied to the problem of calculating the static electric field effects on excitons (Blossey 1970, 1971, Mendez *et al* 1982, Bastard *et al* 1983, Miller *et al* 1985). Numerical estimates recently performed by Rocke *et al* (1997, 1998) and Korotchenkov *et al* (1999) support these assumptions by providing additional evidence which shows that acoustically driven exciton quenching is indeed an electric field effect.

Better insight into this issue is obtained by implementing the field-induced tunnelling ionization of excitons (Rocke *et al* 1998). The authors' prescription is that the tunnelling ionization time τ_{ion} of excitons can be estimated at a given acoustic power and can then be compared with τ_{PL}. For example, the free-exciton PL in InGaAs/GaAs quantum wells is effectively quenched at the SAW power $P = -1$ dB m. The electric field accompanying the SAW is elliptically polarized in the sagittal plane of the wave and an order-of-magnitude estimate of the in-plane electric field $F_{\parallel}$ gives 1 kV cm^{-1} at the given SAW power. Applying a two-dimensional exciton in a static electric field to our problem yields the exciton ionization time (Miller *et al* 1998)

$$\tau_{\mathrm{ion}} \approx \frac{1}{128\sqrt{\pi}} \frac{h}{R_y} \sqrt{\frac{eF_{\parallel}a_B}{R_y}} \exp\left(\frac{8\pi}{3} E_{\mathrm{ex}} \frac{\sqrt{2\mu E_{\mathrm{ex}}}}{heF_{\parallel}} \right) \tag{3.2}$$

where R_y is the Rydberg energy, e is the electron charge and μ is the in-plane reduced effective mass. Inserting appropriate numbers gives $\tau_{\mathrm{ion}} \approx 0.35$ ns (Rocke *et al* 1998) which is smaller than $\tau_{\mathrm{PL}} \approx 0.4$–1.2 ns (Feldman *et al* 1987, Aksenov *et al* 1995), thus indicating that the tunnelling ionization of excitons is physically feasible in acoustic fields.

Better insight emerged during the last few years from the fact that it is now possible to directly observe the driving-induced dissociation of excitons in quantum wells. In one of these experiments, acoustic pump-and-probe techniques (Rocke *et al* 1998) were used in a rather unique combination. By implementing these techniques and employing two SAWs propagating perpendicularly to each other, the authors were able to show that the sheet conductivity of
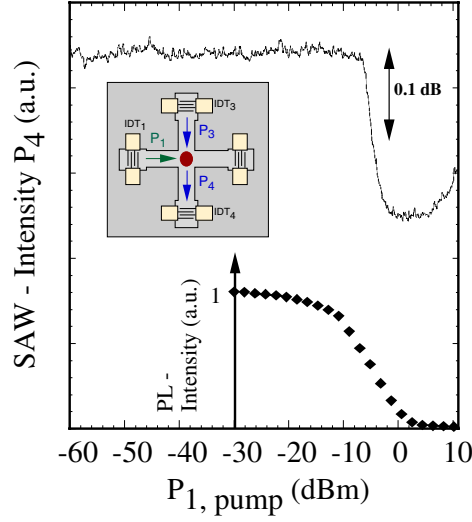
Figure 16. Typical transmitted intensity P_4 of the probe SAW (upper trace) and exciton PL intensity (full circles) versus pump SAW intensity P_1. Upper inset: a schematic diagram of the sample design. The active area of the 10 nm $In_{0.15}Ga_{0.85}As$ QW on the GaAs substrate was etched into a cross-shaped mesa. The pump-and-probe SAWs were generated by applying 420 and 840 MHz frequency voltage to the IDTs IDT_1 and IDT_3, respectively. The transmitted probe SAW was detected by the IDT IDT_4. Optical excitation was performed at the centre of the mesa (dark area). After Rocke *et al* (1998).

free carriers in a QW is affected by the field-induced exciton dissociation (cf upper inset in figure 16). From previous data on the interaction of SAWs with two-dimensional electrons in heterostructures, it is known that SAW attenuation provides a very convenient method of probing free electrons and holes (Wixforth *et al* 1986, 1989, Rocke *et al* 1994, Shilton *et al* 1995, Talyanskii *et al* 1997). The SAW attenuation coefficient Γ_{SAW} can be expressed in terms of the two-dimensional conductivity σ (Wixforth *et al* 1989):

$$\Gamma_{SAW} = k \frac{K_{eff}^2}{2} \frac{\sigma/\sigma_M}{1 + (\sigma/\sigma_M)^2}. \tag{3.3}$$

Here $k = 2\pi/\lambda_{SAW}$ is the wavevector of the SAW, K_{eff} is the effective piezoelectric coupling coefficient for surface waves and σ_M is the critical conductivity yielding maximum attenuation. Hence, the most telling information on the increase in free-carrier concentration is found from the decrease in the intensity of the probe SAW.

This behaviour is clearly seen in the experiment performed by Rocke *et al* (1998) (cf figure 16). At low pumping power levels P_1, the probe SAW remains nearly unaffected by the pump wave, and so does the exciton PL intensity. At higher pumping power level, the authors' model predicts that the decrease in the PL intensity owing to the ionization of excitons should be accompanied by an increase in Γ_{SAW} with increasing σ (equation (3.3)). This increase is expected to cause a drop in the probe SAW intensity which is in perfect agreement with the experimental data exhibited in figure 16. As soon as the pump SAW P_1 reaches -10 dB m, the probe intensity P_4 drops abruptly. Simultaneously, the PL intensity starts to be quenched as illustrated by the lower inset in figure 16.

Rocke *et al* (1998) argued that the probability of exciton ionization due to field-induced tunnelling process is considerably enhanced at pumping powers $P_1 > -6$ dB m which corresponds to a lateral piezoelectric field strength larger than 600 V cm^{-1}. This is consistent
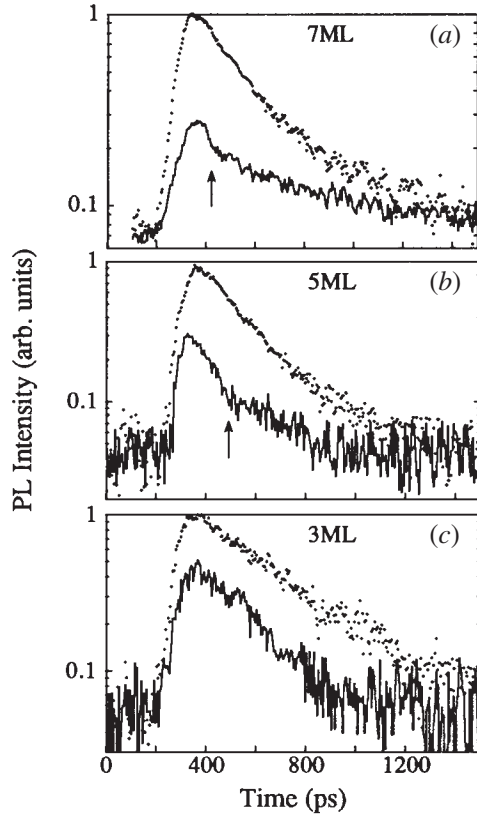
Figure 17. Transient PL intensities from QWs at photon energies 3.052, 3.097 and 3.138 eV for the 7 ML (a), 5 ML (b) and 3 ML (c) wells, respectively, after picosecond excitation at 4.0 eV at $t \approx 200$ ps. The dotted and solid curves correspond to $U = 0$ and 45 V, respectively. After Korotchenkov et al (1999).

with the onset of the transmitted probe intensity observed above $P_1 > -6$ dB m. It should be noticed that, under these conditions, the sheet conductivity σ approaches values which are comparable to or greater than σ_M in equation (3.3). Thus, the onset of the absorption coefficient Γ_{SAW} is well described by the screening of the driving piezoelectric field due to free carriers which reduces the interaction of the probe SAW and the carriers quite considerably.

The exciton relaxation in the driving electric field is commonly visualized by employing time-resolved optical measurement techniques. Time-resolved PL measurements of three different ZnSe/ZnS samples are contrasted in figure 17. The initial decay of the 7 and 5 ML QWs (dotted curves in figures 17(a) and (b), respectively) is well described by the fast exponential decay over an intensity range of about one order of magnitude and exhibits long-lived nonexponential tail emissions which exist on a timescale of nanoseconds, and with an intensity about one decade lower than the fast emission process. For the 3 ML QW, shown in figure 17(c), the dotted curve closely resembles a single-exponential decay over the range from about 400 to 1400 ps. Obviously, for increasing driving amplitudes, the fast-decaying emissions become much faster. They are accompanied by a relative increase in the long-lived tail of the PL at time instants greater than that marked by arrows for the solid curves in figures 17(a) and (b).

The exciton relaxation mechanism discussed above is clearly reflected in the data of figure 17. For example, the spatial coherence of the localized excitons is to a large extent bound to the coherence length L which is determined by lateral dimensions of randomly distributed localized interface states (Akiyama et al 1994). This is clearly manifested by the enhanced τ_{PL} of the 3 ML QW compared to that of the 7 and 5 ML QW (dotted curves in
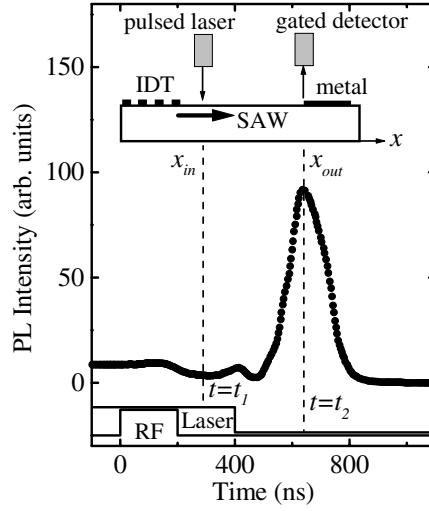
Figure 18. PL intensity of a single 10 nm wide $In_{0.15}Ga_{0.85}As$ QW sandwiched between GaAs buffer and cap layers (upper face in the inset) as a function of time after SAW excitation. The inset illustrates the experimental set-up. The active area of the sample is formed on a (100) GaAs substrate and etched into a mesa with an IDT at its end. At $t = 0$ a 200 ns long rf pulse at $f_{SAW} = 840$ MHz applied to IDT generates a SAW packet with an acoustic power of 13.5 dB m. At $t = t_1$ and $x = x_{in}$, the potential extrema of the SAW are filled with photogenerated electron–hole pairs which are transported at sound velocity to a semitransparent metallized layer at $x = x_{out}$. Here, the deliberate screening of the piezoelectric potential modulation lifts the spatial separation of the carriers and restores radiative recombination at $x = x_{out}$ and $t = t_2$. The duration of the rf pulse and the laser pulse are indicated in the lower part. After Rocke *et al* (1997).

figure 17). The nonexponential decay of the tails in figures 17(a) and (b) may in fact be due to the relaxation of excitons by spatial diffusion within the QW plane. If this is true, the acoustically driven shortening of the PL decays, at time instants smaller than that marked by the arrows in figures 17(a) and (b), gives evidence of an increased E_{ex} (see equation (3.1)), which in turn is supported by the experimentally observed spectral changes exhibited in figure 14. Also, the relocalization of excitons to lower-energy sites by the drift-diffusion motion within the QW may not be important in a thin 3 ML QW, which is evidenced by the absence of a nonexponential tail PL in figure 17(c). In contrast, the driving-induced drift diffusion in the 7 and 5 ML QWs is illustrated by enhanced nonexponential decays in figures 17(a) and (b).

3.2. Implementing photonic memories

The final signatures of acoustically driven PL in QWs, that we wish to discuss here, are those taken with InGaAs/GaAs structures. This implies that we now turn to a somewhat different understanding of the driving effect which is observed in samples with small concentrations of trapping centres. A surprisingly new phenomenon that is conceptually of great importance has been observed by Rocke *et al* (1997). The principal idea of the experiment is shown and described in figure 18. The SAW pulse of 200 ns width is generated by an IDT at time $t = 0$ and travels across the QW plane. At about $t = t_1$, the SAW pulse is centred at the point $x = x_{in}$ where a laser pulse produces e–h pairs. In the absence of driving, exciton luminescence is detected in the QW. The luminescence is effectively quenched by the electric field of the SAW due to the dissociation of excitons into e–h pairs. The dissociated pairs are transferred to the potential wells associated with the travelling wave (see figure 12), and the stored charges are
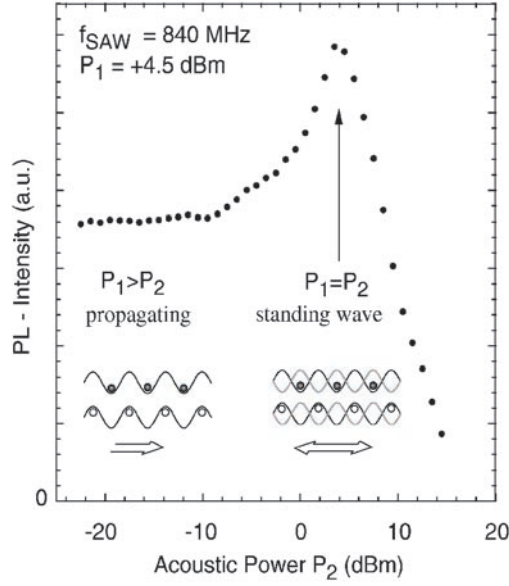
Figure 19. PL intensity as a function of the acoustic power P_2 from IDT$_2$ for a constant acoustic power $P_1 = +5.5$ dB m. The insets illustrate the storage of excitons in the SAW potential. The frequency of the SAWs $f_{SAW1} = f_{SAW2} = 840$ MHz (after Rocke *et al* (1997)).

transported over macroscopic distances at the velocity of the SAW. We thus have a fascinating system with a transport channel of $x_{out} - x_{in} = 1$ mm representing an optical delay line with a charge storage time $t_s \approx 350$ ns provided that the SAW velocity V_{SAW} is 2.865×10^3 m s^{-1}. After the delay time, the SAW pulse reaches the point $x = x_{out}$ where the SAW fields are screened by a metal layer inducing radiative recombination of the e–h pairs which are restored from the SAW packet. As seen in figure 18, strong PL is observed about 650 ns after the SAW pulse is launched, which roughly corresponds to a 350 ns delay between the excitation and the emission of light.

These experiments have been of great importance for testing different models of acoustically driven luminescence and exploring the optical delay lines operating at sound velocities. The interference of two SAWs can provide additional insight into these new results. In this particular case, two SAWs are launched using an opposite pair of IDTs, IDT$_1$ and IDT$_2$, similar to those illustrated in the inset of figure 16. The colliding SAWs create a lateral potential modulation which is oscillating in time and space. The acoustic power, generated by IDT$_1$, levels up to $P_1 = +4.5$ dB m which corresponds to about 50% quenching of the PL intensity. The power P_2 is varied. If $P_2 < P_1$, SAW$_1$ is effectively trapping and transporting the photogenerated electron–hole pairs (left inset in figure 19). When $P_2 = P_1$, the waves interfere and produce a standing-wave pattern (right inset in figure 19). For the standing-wave geometry, the spatial separation of electrons and holes is lifted, which results in enhanced recombination probabilities and recovered PL signals. Further increase in P_2 ($P_2 \approx P_1$) leads to decreased PL intensity as long as SAW$_2$ effectively reduces the recombination probability by spatially separating the e–h pairs. This is clearly seen in figure 19 at $P_2 \gtrsim 5$ dB m.

These observations provide a better understanding of acoustically tunable lateral potential modulation in the plane of a quantum well and suggest storage of light for an appreciable amount of time. In a storage cell, light energy can be locally accumulated and stored for microseconds by converting it into spatially separated electron–hole pairs. At a given time, the light may be re-emitted from the cell in a short flash by triggering the radiative recombination processes. The variable delay times can be tailored by the piezoelectric potential of the SAW or by a low-
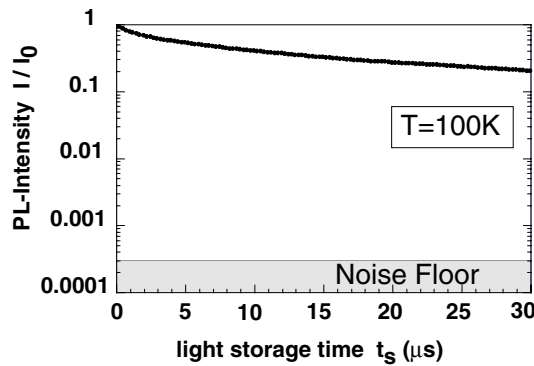
Figure 20. Time-delayed PL intensity I versus storage time t_s in a GaAs/AlAs quantum well. I_0: PL intensity at $t_s = 0$. From Zimmermann *et al* (1999).

voltage-induced lateral electrostatic potential implemented on a patterned chip (Zimmermann *et al* 1999). Similarly to electronic memory devices, the cell should act as an optical memory for storage or delay of selected optical bits.

There is a problem for storage over an arbitrarily chosen time period due to the gradual loss of the photogenerated and trapped carriers along the travelling distance, because of nonradiative recombination of the storage charge. This question has been extensively addressed previously (Rocke *et al* 1997, Zimmermann *et al* 1999) and large storage times, in excess of several tens of microseconds, are currently considered to be feasible. The supporting evidence is given in figure 20. Shown here is the intensity of the delayed light flash as a function of the storage time t_s. In this experiment, a low-intensity photonic signal was accumulated in the cell over long time intervals and then released in a single bright short flash. This data array was restricted to storage times of about 35 μs, and the released signal was well above the noise level. On optimizing the sample design, the storage time seems to grow, and it is therefore not unrealistic to believe that $t_s \approx 100$ μs and even higher values can be obtained.

These experiments had a pronounced impact on our intention of further exploiting the technique developed for optical signal processing.

3.3. Pumping microcavities

Recent progress in the development of nanometre-sized semiconductors has led to numerous studies of quantum wells, quantum wires and quantum dots as candidates for laser media use. Among these, quantum wires and quantum dots are of particular interest because they can be completely embedded in micrometre-sized optical microcavities. Due to quantum confinement, the optical emission strength of a low-dimensional semiconductor is concentrated into a narrow frequency range, and, because of a wavelength-sized optical microcavity, all the light is channelled into a single emission mode.

It is therefore presumed that the acoustically driven modulation superlattices described above allow a completely new way of integrating conventional optical microcavities and quantum wire (or even quantum dot) structures which will result in a highly efficient light emission. By tuning the frequency of the driving wave, the emission parameters are easily varied.

Since the SAW is able to deliver electrons and holes periodically, it is crucial to realize that this technique can be used to pump periodically a localized array of quantum dots or even a single dot. The first insights into this topic were provided by Wiele *et al* (1998). The principal finding is pictured in figure 21. A quantum dot is achieved by a stressor that provides a local potential minimum in the quantum well underneath. A 10–30 nm sized stressor dot is believed to result in a potential depth of about 100 meV for electrons and 50 meV for holes.
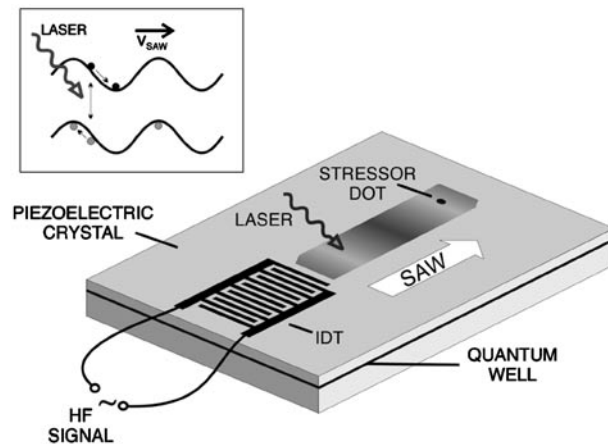
Figure 21. A schematic illustration of acoustically pumped quantum dots showing a quantum well on a piezoelectric crystal (for example, an InGaAs QW on a GaAs substrate) and a stressor dot which may be formed e.g. by InP. Laser-excited excitons in the quantum well are dissociated by high-frequency piezoelectric fields produced by the SAW. The released electrons and holes are then stored in the moving potential of the SAW, as shown in the inset (after Wiele *et al* (1998)).

Using our previous ideas, we can now go further by assuming that the dot is so small that only one electron level and one hole level are left, thus producing a single exciton state. For sufficiently high SAW amplitudes, laser-generated excitons in the quantum well are dissociated by the piezoelectric field which can be as high as 500 V cm^{-1} or typically 50–150 meV in energy units. The carriers are trapped in the moving potential of the SAW resulting in a series of equally spaced quantum wires moving in the plane of the quantum well. The occupation of the wires with electrons and holes depends on the laser power and SAW intensity, and was reported to achieve 10^3–10^4 carriers per wire. When the SAW crosses the stressor dot, a carrier may drop into it. If only one carrier (electron or hole) is already present in the dot, the exciton state is formed by capturing the missing carrier from the moving wires.

Given that the quantum wires are equally spaced in the travelling potential of the SAW, the wave delivers a periodic sequence of electrons and holes. For subsequent exciton recombination in the dot, two different regimes are identified (Wiele *et al* 1998) depending on the quality of the optical cavity. In a first application of the pumping mechanism presented, one could suggest a nonperfect single-mode cavity. When the cavity damping rate is greater than the exciton–light field coupling constant, a train of equally spaced photons would arise. As a result, perhaps, the combination of acoustically driven regular pumping and a high-quality optical cavity could entail using photon statistics, which has been attributed to atomic microlasers (see e.g. Filipowicz *et al* (1986), Puri *et al* (1996)).

Hence, acoustically driven lasing does currently have theoretical support in the form of a two-level pumped stressor dot (Wiele *et al* 1998). The combination of physical acoustics, quantum dots and cavity physics would initiate an exciting field of research where continued progress could be expected in the immediate future.

4. Future prospects

Major progress has been made in the past three years by recognizing the unique properties of acoustic techniques for driving the luminescence of semiconductors. Work on acoustically

induced emission of light in granular solids is motivated by the continuous development of sonoluminescence techniques in liquids, which increase our understanding in both research fields. The implications on the underlying mechanisms, involved in many of the basic ideas of acoustic driving techniques, can be quite far reaching and, hence, will stimulate new technologies and, thus, increase our insight into this particular field. These new technologies include the fundamental properties of grain slip motions, intergrain interactions and particle packing events which are relevant to the classical scope of physics as well as to many technologies, such as transportation, processing and handling of particular solids. More work still needs to be done beyond the formal description of such links as have been highlighted here. In particular, surface studies obviously do not reveal the full complexity of granular movements, so the question of how much insight one may obtain from the dynamics of the inner layers of a granular system with the techniques developed remains unanswered and demonstrates their limitations. On the theoretical side, a number of uncertainties remain, including the fundamental problem of whether or not the sonoluminescence effect in liquids and acoustically induced luminescence in granular matter can indeed be treated on the same footing. In analogy to the critical behaviour of nonequilibrium systems, applications of the techniques presented are expected to lead to novel insights in probing the fractal behaviour of nature.

The recently documented acoustically driven emission of light in quantum wells has been carried out in previously uncharted territory. The concept of unipolar charge transport by SAW (Hoskins *et al* 1982) has proven to be important for high-speed signal processing (Tanski *et al* 1987). The present advances of ambipolar charge transport with subsequent recombination at dramatically prolonged times extends the arsenal of techniques used to probe light emission and offers a new way of tailoring multilayer structures. Many applications need an optical memory for storage and delay of optical bits. Ideally, this should be an integrated device implemented on a chip in which an incoming signal could be stored for a chosen time. The key physics of a potentially very efficient storage cell utilizing acoustic waves has already been developed and summarized in the present review.

The ideas as they stand are applicable in a broader view. At first glance, it seems most probable that strong interband optical transitions are linked to direct-band-gap semiconductors with short radiative lifetimes, whereas long radiative lifetimes imply indirect-band-gap semiconductors with substantially reduced interband absorption. This suggests reconsidering the doping of superlattices (Döhler *et al* 1981) in order to combine strong interband absorption with long radiative lifetimes. Currently, there seems to be a new thinking in band-gap engineering which employs superlattices acoustically modulated in the plane of a quantum well, thus using the advantages of strong interband absorption as well as extremely long lifetimes.

We have also illustrated the ideas of acoustically pumped lasing in the context of the exciton emission in a quantum dot. Their validity should now be tested in experiments which could pave the way for new mechanisms of acoustically driven lasing effects.

We believe that one of the challenges for the future is to find appropriate ways of exploiting the power of acoustic driving techniques.

Acknowledgments

References

Akiyama H, Koshiba S, Someya T, Wada K, Noge H, Nakamura Y, Inoshita T, Shimizu A and Sakaki H 1994 *Phys. Rev. Lett.* **72** 924

Aksenov I, Aoyagi Y, Kusano J, Sugano T, Yasuda T and Segawa Y 1995 *Japan. J. Appl. Phys.* **34** L547

Alzetta G, Minnaja N and Santucci S 1962 *Nuovo Cimento* **23** 910

Auld B A 1990 *Acoustic Fields and Waves in Solids* (Malabar, FL: Krieger)

Barber B P, Hiller R A, Löfstedt R, Putterman S J and Weninger K R 1997 *Phys. Rep.* **281** 65

Bastard G, Mendez E E, Chang L L and Esaki L 1983 *Phys. Rev.* B **28** 3241

Bideau D and Dodds J A (ed) 1991 *Physics of Granular Media* (*Les Houches Series*) (New York: Nova Science)

Blossey D F 1970 *Phys. Rev.* B **2** 3976

Blossey D F 1971 *Phys. Rev.* B **3** 1382

Colic M and Morse D 1998 *Phys. Rev. Lett.* **80** 2465

Crum L A 1994 *Phys. Today* **47** 22

Czyzyk M T and Mueller F M 1983 *J. Phys. C: Solid State Phys.* **16** 5255

Damen T C, Shah J, Oberli D Y, Chemla D S, Cunningham J E and Kuo J M 1990 *Phys. Rev.* B **42** 743

Döhler G H, Künzel H, Olego D, Ploog K, Ruden P and Stolz H J 1981 *Phys. Rev. Lett.* **47** 864

Eberlein C 1996 *Phys. Rev. Lett.* **76** 3842

Feldman J, Peter G, Göbel E O, Dawson P, Moore K, Foxon C and Elliott R J 1987 *Phys. Rev. Lett.* **59** 2337

Filipowicz P, Javanainen J and Meystre P 1986 *Phys. Rev.* A **34** 3077

Graff K F 1991 *Wave Motion in Elastic Solids* (New York: Dover)

Haff P K 1983 *J. Fluid Mech.* **134** 401

Haroche S and Kleppner D 1989 *Phys. Today* **42** 24

Hegarty J, Sturge M D, Weisbuch C, Gossard A C and Wiegmann W 1982 *Phys. Rev. Lett.* **49** 930

Hoskins M J, Markoc H and Hunsinger B 1982 *Appl. Phys. Lett.* **41** 332

Huang M Z and Ching W Y 1993 *Phys. Rev.* B **46** 9449

Jaeger H M, Nagel S R and Behringer R P 1996 *Rev. Mod. Phys.* **68** 1259

Jenkins J T and Savage S B 1983 *J. Fluid Mech.* **130** 187

Korotchenkov O A and Goto T 1997 *Phys. Rev.* B **56** 13 646

Korotchenkov O A and Goto T 1999 *J. Appl. Phys.* **85** 1153

Korotchenkov O A and Grimmeiss H G 1995 *Phys. Rev.* B **52** 14 598

Korotchenkov O A, Yamamoto A, Goto T, Cho M-W and Yao T 1999 *Appl. Phys. Lett.* **74** 3179

Landau L D and Lifshitz E M 1986 *Theory of Elasticity* 3rd edition (Oxford: Pergamon)

Langford S C, Dickinson J T and Jensen L C 1987 *J. Appl. Phys.* **62** 1437

Mendez E E, Bastard G, Chang L L, Esaki L, Morkoc H and Fischer R 1982 *Phys. Rev.* B **26** 7101

Miller D A B, Chemla D S, Damen T C, Gossard A C, Wiegmann W, Wood T H and Burrus C A 1985 *Phys. Rev.* B **32** 1043

Nyborg W L M 1965 *Physical Acoustics* vol II-B, ed W P Mason (New York: Academic) p 265

Onoda G Y and Liniger E G 1990 *Phys. Rev. Lett.* **64** 2727

Ostrovskii I V 1981 *Pis. Zh. Eksp. Teor. Fiz.* **34** 463 (Engl. transl. 1981 *JETP Lett.* **34** 467)

Ostrovskii I V and Das P 1997 *Appl. Phys. Lett.* **70** 167

Ostrovskii I V and Korotchenkov O A 2000 *J. Phys. Chem. Solids* **61** 1321

Ostrovskii I V, Korotchenkov O A, Goto T and Grimmeiss H G 1999 *Phys. Rep.* **311** 1

Ostrovskii I V and Lysenko V N 1982 *Fiz. Tverd. Tela* **24** 1206 (Engl. transl. 1982 *Sov. Phys.–Solid State* **24** 682)

Pankove J I 1971 *Optical Processes in Semiconductors* (New York: Dover)

Picard J 1676 *Mem. R. Acad. Sci.* **2** 202

Polland H-J, Schultheis L, Kuhl J, Göbel E O and Tu C W 1985 *Phys. Rev. Lett.* **55** 2610

Powell R C and Soos Z G 1975 *J. Lumin.* **11** 1

Prevenslik T V 2000 *J. Lumin.* **87–89** 1210

Puri R P, Haake F and Forster D 1996 *J. Opt. Soc. Am.* B **13** 2689

Ridley B K 1990 *Phys. Rev.* B **41** 12 190

Rigby N E and Allen J W 1988 *J. Phys. C: Solid State Phys.* **21** 3483

Rocke C, Govorov A O, Wixforth A, Böhm G and Weimann G 1998 *Phys. Rev.* B **57** R6850

Rocke C, Manus S, Wixforth A, Sundaram M, English J H and Gossard A C 1994 *Appl. Phys. Lett.* **65** 2422

Rocke C, Zimmermann S, Wixforth A, Kotthaus J P, Böhm G and Weimann G 1997 *Phys. Rev. Lett.* **78** 4099

Runge E, Schulzgen A, Henneberger F and Zimmermann R 1995 *Phys. Status Solidi* **188** 547

Ryvkin S M 1965 *Phys. Status Solidi* **11** 285

Santos P V and Hey R 2000 *Physica* E **7** 559

Schwinger J 1992 *Proc. Natl Acad. Sci. USA* **89** 4091

Shilton J M, Mace D R, Talyanskii V I, Simmons M Y, Pepper M, Churchill A C and Ritchie D A 1995 *J. Phys.: Condens. Matter* **7** 7675

Sogawa T, Santos P V, Zhang S K, Eshlaghi S, Wieck A D and Ploog K H 2001 *Phys. Rev.* B **63** R121307

Streibl M, Wixforth A and Gossard A C 1999 *Appl. Phys. Lett.* **75** 4139

Tabib-Azar M and Das P 1987 *Appl. Phys. Lett.* **51** 436

Talyanskii V I, Shilton J M, Pepper M, Smith C G, Ford C J B, Linfield E H, Ritchie D A and Jones G A C 1997 *Phys. Rev.* B **56** 15 180

Tanski W J, Merritt S W, Sacks R N and Cullen D E 1988 *Appl. Phys. Lett.* **52** 18

Thadhani N N, Graham R A, Royal T, Dunbar E, Anderson M U and Holman G T 1997 *J. Appl. Phys.* **82** 1113

Thornton C (ed) 1993 *Powders and Grains* (Rotterdam: Balkema)

Tong D D and Goede O 1983 *Phys. Status Solidi* b **120** K145

Turvey K and Allen J W 1973 *J. Phys. C: Solid State Phys.* **6** 2887

Umlauff M, Hoffmann J, Kalt H, Langbein W, Hvam J M, Scholl M, Söllner J, Heuken M, Jobst B and Hommel D 1998 *Phys. Rev.* B **57** 1390

Viktorov I A 1967 *Rayleigh and Lamb Waves* (New York: Plenum)

Visser M, Liberati S, Belgiorno F and Sciama D W 1999 *Phys. Rev. Lett.* **83** 678

Walton A J 1977 *Adv. Phys.* **26** 887

Walton A J and Reynolds G T 1984 *Adv. Phys.* **33** 595

Wiele C, Haake F, Rocke C and Wixforth A 1998 *Phys. Rev.* A **58** R2680

Wixforth A, Kotthaus J P and Weimann G 1986 *Phys. Rev. Lett.* **56** 2104

Wixforth A, Scriba J, Wassermeier M, Kotthaus J P, Weimann G and Schlapp W 1989 *Phys. Rev.* B **40** 7874

Yao T, Fujimoto M, Chang S K and Tanino H 1991 *J. Cryst. Growth* **111** 823

Zachau M, Kash J A and Masselink W T 1991 *Phys. Rev.* B **44** 8403

Zhuravlev K S, Petrov D V, Bolkhovityanov Yu B and Rudaja N S 1997 *Appl. Phys. Lett.* **70** 3389

Zimmermann S, Wixforth A, Kotthaus J P, Wegscheider W and Bichler M A 1999 *Science* **283** 1292